Chapter 3

The Formation and Migration of Molten Inclusions in Silicon

Arkady Skvortsov

Additional information is available at the end of the chapter

http://dx.doi.org/10.5772/67787

Abstract

The mechanisms of formation and migration of molten inclusions in silicon are described. Consideration of them is necessary for development of technological approaches to formation of conducting regions (characteristic sizes of 10 μm–30 nm) and doped conducting channels in silicon. The problem of formation of local conducting regions is topical, e.g., for single electronics. It is known that sizes of a "Coulomb island" (about 10 nm) present difficulties to modern technologies. That is why the development of alternative procedures to form a "Coulomb island" (in particular, those based on electromigration of molten regions in semiconductor bulk) is a topical problem. Besides, high heat loads on the "classical" silicon structures, owing to specific character of their work (operating current densities may be as high as $j \sim 10^9$–10^{10} A/m^2), promote their active degradation. The appearing molten regions coagulate into drops and are displaced by a current along the electric field lines. Therefore, a detailed analysis of the mechanisms of inclusions formation and migration in silicon will make it possible to predict more accurately the "critical" modes of silicon structures operation (e.g., in power electronics). The main mechanisms of molten inclusions formation (contact melting in a metal-semiconductor system, decomposition of supersaturated solid solutions in heavily doped semiconductors) are considered, as well as the procedures to form and control mobility of such objects: electric current, temperature gradient, structural inhomogeneities, etc. The problems of molten inclusions migration in silicon single crystals occurring in electric field with contact melting electric transport of melt components and thermoelectric effects at interphase boundaries are considered in detail. The molten region is moving along the electric field lines, thus enabling to exert control over the trajectory of its motion. The results of author's original investigations on formation and migration of molten silver- and aluminum-based inclusions in silicon are presented, as well as the experimental data by other authors. The main migration mechanisms related to melting-crystallization processes at

interphase boundaries and components diffusion through the melt region are discussed in detail. The problems to defect formation in silicon after crystallization of inclusions are also considered.

Keywords: silicon single crystals, contact melting, crystallization, melt inclusion, formation of molten regions in a metal-semiconductor system, electromigration of inclusions by the melting-crystallization mechanism, diffusion in the melt, gradients of concentration and temperature, formation of structural defects in silicon single crystals with inclusions

1. Introduction

Formation and dynamics of impurities in semiconductors as melt regions occur, as a rule, when the critical operating conditions for power semiconductor devices (transistors, Peltier elements, etc.) are reached [1–3]. In this case, as is known [4, 5], the near-contact regions and metal-semiconductor contacts may heat up to temperatures over the melting points for eutectics of relatively fusible systems (Al-Si, Ag-Si, Au-Si; the melting point for Au-Si eutectic Te = 370°C).

To illustrate, during operation of a thermoelectric generator for automobile internal-combustion engines, certain modules or their parts may be heated for a short time to temperatures over 330°C [6]. The result can be fusion of structure fragments and their failure. And this happens despite equalizing of temperature field (provided with the construction of heat-exchange apparatus) at the hot side of thermoelectric modules [6]. Obviously, failure of electric contact in a thermoelectric module because of overheating will lead to failure of the whole system, thus considerably reducing the efficiency of thermoelectric generator.

During operation of such devices, a direct electric current consumed by the resistive load is flowing through each module. At overheating and beginning of fusion, the current flows through the liquid phase-crystal contact. This makes it necessary to study the electromigration processes at the semiconductor surface and in the bulk involving melt regions that are proceeding under the action of direct and pulse currents. In those cases, migration of the produced liquid phase in electric field is possible in the system studied. The field of crystal structural nonuniformity (gradient of dislocation density) also can promote migration of the melt regions [7, 8]. These are just the above factors that cause the interest of researchers in the electromigration processes at the semiconductor surface and in the bulk involving melt regions [9].

As a rule, migration of liquid inclusions in semiconductors is related to transfer of matrix atoms from one inclusion boundary to another through the inclusion itself. An inclusion migrates because the matrix atoms are dissolving at the forward inclusion wall, then they are diffusing through the inclusion and at last become deposited onto the matrix at the back wall, with formation of new atomic layers. In the case of liquid inclusions, solubility of matrix atoms in the inclusion and the coefficient of diffusion of these atoms in the inclusion bulk are sufficiently high, so such a migration mechanism is crucial [10, 11].

http://dx.doi.org/10.5772/67787

With such a mechanism, flowing of electric current through the liquid phase-crystal contact is accompanied by Peltier heat release at the one interphase boundary and absorption at the other interphase boundary: $\pm Q_p = Pjt$. (Here P is the Peltier coefficient at the melt-crystal interface, j is the current density, t is the time of current action.) This leads to variation of concentrations at the inclusion walls and requires accounting for thermoelectric effects in the course of mass transfer. Besides, one should also take into account the effect of electromigration that creates concentration nonuniformity near the interphase boundaries, depending on the value and sign of the effective charge Z^* of semiconductor atoms in the melt [10, 11].

When determining the predominant role of the above mechanisms, one should note that for inclusions of sizes

$$\ell \gg \sqrt{\frac{D\tau}{\pi}}, \tag{1}$$

(τ is the current pulse duration), only the contribution from Peltier heat is significant at migration.

A qualitative experimental confirmation of this statement was made for elementary semiconductors of *p*- and *n*-type. At pulse duration $\tau = 150$ μs and pulse height $I = 6 \times 10^3$ A, migration of drops of the Al, Ga, Ag melt occurred towards anode and was determined by the thermoelectric effects at the interphase boundaries. In the stationary regime, inversion of drop velocity was observed (the drops moved towards the negative electrode). This indicated the predominant role of electromigration. Unfortunately, application of nonstationary heating of semiconductor and surface migration only prevented obtaining dimensional dependence of migration velocity.

To determine the nature of mass transfer, let us assess the path velocity in accordance with the known mechanisms [12].

In the case of a vacancion mechanism of inclusion transfer, a vacancy current in the matrix creates a counter current and an equal current of matrix atoms. In this case, the speed of inclusion migration, w, can be expressed by the following ratio:

$$w = -\frac{2(\rho_s - \rho_\ell)}{2\rho_s + \rho_\ell} \frac{D_s e Z^*}{fkT} E_\infty. \tag{2}$$

Here, D_s is the self-diffusion coefficient of semiconductor atoms, E_∞ is the density of the electric field away from the inclusion, f is a correlation factor, and ρ_s and ρ_ℓ are the electrical conductivities of the matrix and inclusion, respectively.

The effective charge of the atoms in a semiconductor matrix is known to be negative. This makes the activated atoms of the semiconductors move toward the anode, while vacancies move toward the cathode. By occupying vacancies at the leading edge, atoms of inclusions ensure that the edge is pushed toward the positive electrode. Therefore, inclusions should be displaced against the electric field lines, a prediction that is inconsistent with the experimental results. In addition, the assessed velocity, w, for aluminum inclusions in silicon is $w = 5 \times 10^{-15}$ m/s in the case where the silicon self-diffusion coefficient is $D_s = 3 \times 10^{-18}$ m^2/s (temperature of T~1043 K) [13]. Here, $E_\infty = 10$ V/m, $\rho_\ell = 2 \times 10^{-6}$ Ω·m, $\rho_{ol} = 10^{-5}$ Ω·m, $Z^* = -10$, $f = 0.8$, and $R = 8.31$ J/(K·mol). Both the operator of the migration velocity w and its seventh-order (10^7)

lower value are inconsistent with the experiment. Therefore, the contribution of this mechanism can be considered insignificant.

As the molten zones are displaced, surface diffusion [12] is visible only for low-conductivity inclusions. Its importance obviously increases at low temperatures, when the surface/bulk diffusion ratio is high. The velocity, w, determined by this mechanism can be assessed using the following equation:

$$w = -3\frac{D_s' ae Z^*}{HfkT}E_\infty, \tag{3}$$

where $D_s' = 10^{-12}$ m^2/s, $a = 5 \times 10^{-5}$ m, $H = 10^{-4}$ m, and $T = 1043$ K. The expected velocity value determined by this mechanism is three times lower than the experimental value.

The movement of inclusions in the electric field associated with the current of matrix atoms in bulk inclusions can be rather fast if the melted material is a conductor. A theoretical estimate of w for this case can also be provided using the known ratios [12], assuming targeted transport of matrix atoms in the melt under the electric transport effect.

When $T = 1043$ K and $j = 10^6$ A/m^2, the displacement velocity for the diffusion and kinetic modes equals

$$w = -\frac{V_s}{V_\ell}\left[\frac{3\rho_s}{2\rho_\ell + \rho_s}\right]\frac{De Z^* C}{fkT\ell}E_\infty = 2 \cdot 10^8 \text{ m/s}, \tag{4}$$

$$w = -V_s\left[\frac{3\rho_s}{2\rho_\ell + \rho_s}\right]\frac{\beta e Z^* C\ell}{fkT}E_\infty = 4 \cdot 10^8 \text{ m/s}. \tag{5}$$

From this point onward, V_s and V_ℓ represent the atomic volumes of the matrix and inclusion, respectively.

The theoretical estimates, w, for the diffusion and kinetic modes are consistent with the experiment in terms of quality. However, the ratios used in this case do not show the complexity of the phenomena that occur when current passes through the inclusion. One can easily notice that Eq. (4) results in a size dependence of approximately $w = 1/\ell$, while Eq. (5) yields $\frac{w}{j} = \text{const} \cdot \ell$, which does not fully describe the experiment. The observed discrepancy in the data obtained through calculation and experiment requires that more than just electric transport should be taken into account in the case of targeted migration.

Therefore, by analyzing the movement of secondary phases in the bulk semiconductor (**Figure 1**), we take into account the fact that movement is performed not only by means of electric transport but also under the influence of thermoelectric phenomena (the Peltier effect) at the interface between the liquid inclusion and solid phase [14–16].

If targeted migration is determined via dissolution-crystallization at the phase interfaces (kinetic control $\beta\,\delta \ll D$), then the equation for w takes the following form [17, 18]:

$$\frac{w}{j} = = -\frac{V\beta\overline{C}}{N_A}\left(\frac{\delta\rho e Z^*}{kT} + \frac{V P_{LS} L}{N_A 2\lambda k T^2}\cdot\ell\right). \tag{6}$$

In the case of diffusion control ($\beta\,\delta \ll D$), the equation becomes

$$\frac{w}{j} = -\frac{VD\overline{C}}{N_A}\left(\frac{\rho e Z^*}{kT} + \frac{V P_{LS} L}{\delta N_A 2\lambda k T^2}\cdot\ell\right). \tag{7}$$

http://dx.doi.org/10.5772/67787

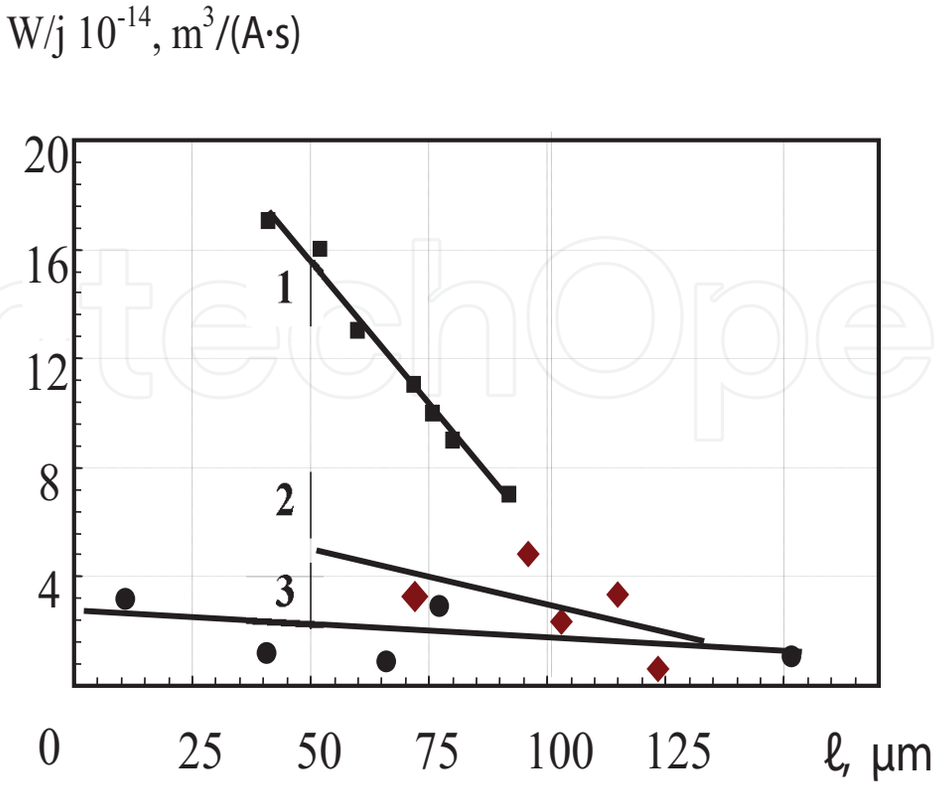

Figure 1. Dimensional dependence of migration of Al-Si inclusions in the bulk of single crystalline silicon at T = 1073 K at flowing: 1—direct current of 12 A; 2—rectangular current pulses of height I_{max} = 24 A and duration τ = 300 μs; 3—I_{max} = 24 A and τ = 900 μs.

where P_{LS} is the Peltier coefficient of the melt-crystal interface, V is the specific volume of the melt, $\overline{C}$ and D are the equilibrium density and diffusion coefficient of the conductor molecules in the melt, respectively, N_A is Avogadro's number, δ is the thickness of the diffusion layer at the phase interface, L is the temperature of the transition of one volumetric unit of the solid phase into the melt, and λ_e is the thermal conductivity coefficient usually calculated according to the Wiedemann-Franz law.

2. Materials and methods

The experiments were performed in a vacuum chamber for silicon (n-type, resistivity of 10 Ω·cm) specimens that were previously cut into 4 × 4 × 15 mm blocks (**Figure 2**). After lapping with M-15 micropowder and with ACM-5 diamond paste, the specimens were treated with ethanol and then were clamped between two tantalum electrodes by the procedure described in Refs. [10, 11] in a quartz electric resistance furnace. A 5 mm thick graphite spacers were put between the specimen and electrodes to prevent their contact interaction. The electrodes were connected to the dc source through an ammeter using copper wires. When performing experiments with current pulses, we used a rectangular pulse generator. The pulse duration and height were τ = 100–1000 μs and I = 5–30 A, respectively.

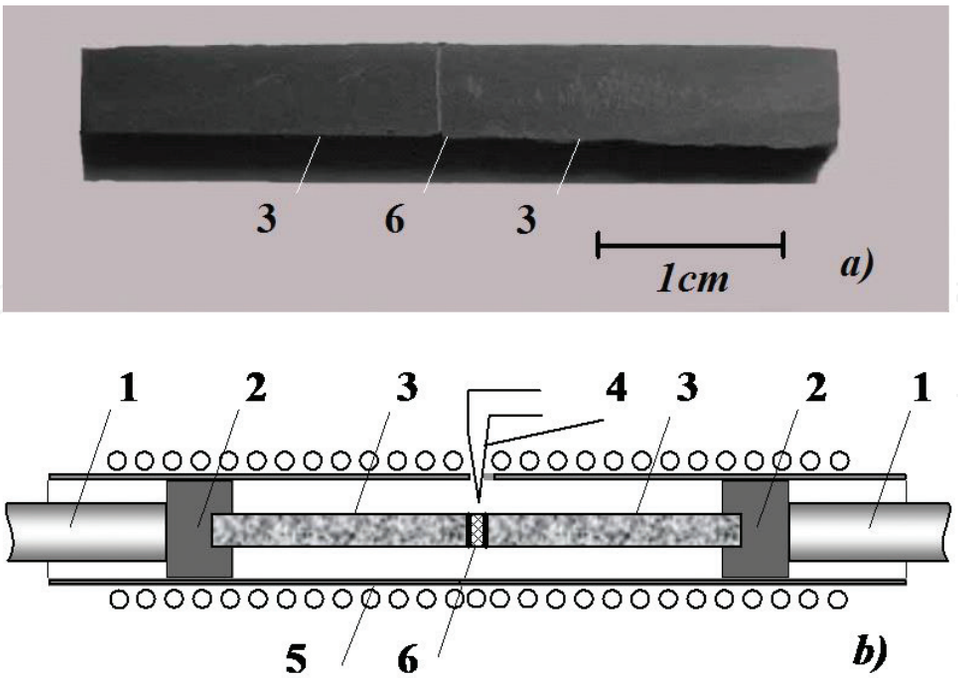

Figure 2. (a) Visual appearance of samples and (b) annealing configuration: 1—electrodes; 2—graphite interlayers; 3—samples; 4—thermocouple; 5—quartz-based resistive furnace; 6—metal film.

At migration in the bulk, an aluminum plate (mass of 0.6–0.9 mg) was put between the {111} planes of two specimens. Then they were heated up to a temperature close to the experiment one (T = 1000–1123 K). The experiment temperature was determined by the net effect from the space heater and electric current flowing through the specimen.

In the course of experiment performance, the temperature of the specimen was determined either using the thermocouple method or from the specimen luminosity. In the latter case, the temperature regimes in the experiments were registered with a pregraduated photocell located on one of the eyepieces of a high temperature microscope. The temperature measurement error was not more than ±10%. The distribution of temperature T and concentration C of semiconductor atoms (dissolved in inclusion) during migration of the melt region are presented in **Figure 3**.

An occurrence of melt regions in the silicon matrix bulk at stationary electric annealing is related to formation of an alloy between an Al film and Si single crystal. This mechanism obeys the reaction-diffusion law: a new phase is formed that was not found before interaction between components. Its growing is given by the following expression [15]:

$$x = 2\beta\sqrt{D\,\tau_k}. \tag{8}$$

Here D is the reaction-diffusion coefficient; β is an argument of the Kramp function that is determined from the diagram of phase equilibrium. Thereby, a melt film is formed at the metal-semiconductor interface as the proper temperature is reached. Thermodynamic

http://dx.doi.org/10.5772/67787

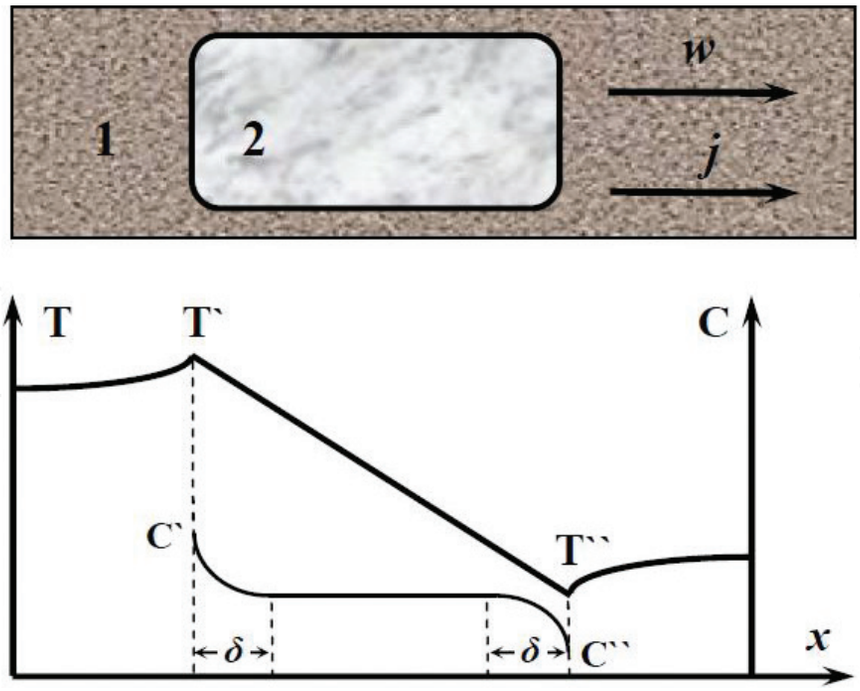

Figure 3. Schematic of migration of melt region: 1—semiconductor matrix; 2—melt inclusion. Distribution of temperature T and concentration C of semiconductor atoms (dissolved in inclusion) during migration of the melt region.

instability of the film promotes its dispersion into drops. The inclusions generated in such a way drift in an electric field.

An analysis of numerous experimental data obtained for the Al-Si system showed that, in the course of migration, melt inclusions are faceted by specific crystallographic planes that shape inclusions into a distinguishing feature (**Figure 4**). In this case, the electric current flowing through the inclusion does not distort the form of drifting regions.

To determine crystallographic indices of the faceting planes at migration of the Al-Si system, the equation of structural crystallography for a cubic lattice [12] was used:

$$\cos\varphi = \frac{h_1 h_2 + k_1 k_2 + l_1 l_2}{\sqrt{h_1^2 + k_1^2 + l_1^2} + \sqrt{h_2^2 + k_2^2 + l_2^2}} \quad (9)$$

Here φ is the angle between the planes; h_i , k_i, and l_i are the indices of crystallographic planes. According to the experimental data, an angle φ between the {111} plane and those with unknown indices $\{h_2,k_2,l_2\}$ is 35° or 145° for which $\cos\varphi$ = +0.819. A good agreement between the experimental and theoretical values of $\cos\varphi$ can be obtained if (110) and $(\bar{1}\bar{1}0)$ will correspond to the indices h_i , k_i, and l_i: substitution of the above values in Eq. (4) gives $\cos\varphi$ = +0.821.

The inclusion size and depth of inclusion penetration in the matrix from the starting position were determined by sequential removal of N layers (at every 5–10 μm) [10, 11, 13] with subsequent identification of inclusions using an optical microscope.

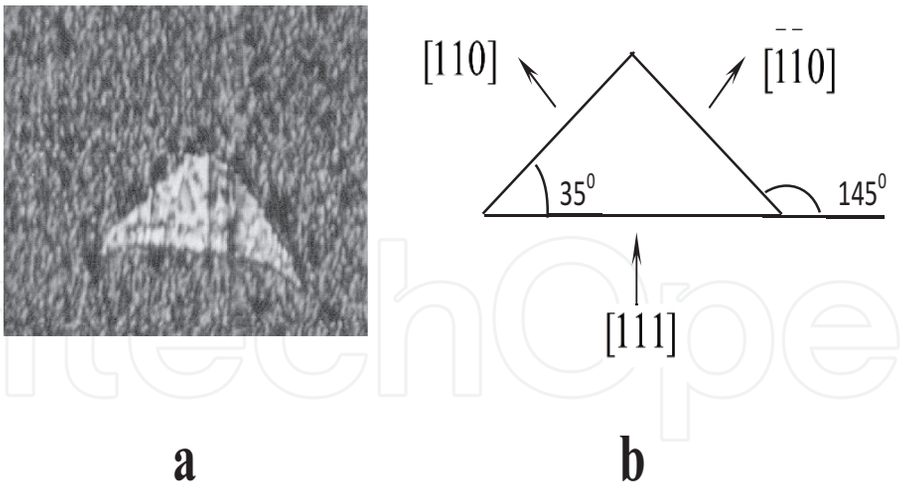

Figure 4. A pattern of Al-Si inclusion in single crystalline silicon. The section plane: ⊥(111). Magnification: ×200.

3. Analysis of experimental results

The typical results of investigations are presented in **Figure 4**. As before [10, 11, 14], the dimensional dependence of migration velocity is linear. To identify the origin of driving forces that determine inclusion migration in electric field in the case of predominance of transfer processes in inclusion bulk, let us use Eq. (7).

For a stationary electric annealing (1, **Figure 4**), Eq. (7) agrees fully with experiment if P is considered negative and Z^* is considered positive. At pulse current action, the character of dimensional dependence is changed—see Eqs. (3) and (4), **Figure 4**. Reduction of pulse duration leads to increase of velocity for inclusions of the same size. We relate the main responsibility for the observed variations to reduction of the contribution from electromigration.

Indeed, at $P < 0$ the concentration nonuniformity at interphase boundaries is provided by heat release (absorption) Q_p at the cathode (anode) interphase boundary. This promotes inclusion migration because of melting-crystallization at the interphase boundaries along the electric field lines (just as observed in the experiment). Electromigration ($Z^* > 0$) will produce the opposite gradient, thus reducing $\partial C/\partial x$ of the thermoelectric origin.

So, migration of inclusions at stationary electric annealing of Si crystals is determined by heat release at the interphase boundaries that ensures migration of inclusions toward the negative electrode. Electromigration produces the opposite gradient, which decreases the resulting inclusion velocity. The smaller the length of electric current pulses is, the weaker is their effect on reduction of the contribution from electromigration to the resulting inclusion velocity. This shows itself most clearly at pulse duration τ = 300 μs.

http://dx.doi.org/10.5772/67787

The crystallization of molten inclusions in a semiconductor is accompanied by active formation of defects, namely dislocations. The results of independent research (**Figure 5**) and our studies (**Figure 6**) both indicate the formation of dislocations during the crystallization of the molten zone near the crystallization front.

During the crystallization of single silicon crystals, the area occupied by the drop will contain approximately 10% of the extrinsic stacking (interstitial) atoms because of the higher (approximately ~10%) density of liquid silicon compared with a single crystal [19]. At a certain drop size, extrinsic stacking atoms may transform into a dislocation loop (**Figure 6**).

The shape of second-phase inclusions depends not only on the crystallographic properties of the matrix but also on the reactivity of the melt. If there is an impurity near the drop, it will diffuse into the liquid and dissolve within it because of the higher solubility of impurities in a liquid phase. In this case, the infrared light-absorption coefficient will increase and the molten zone will be stabilized.

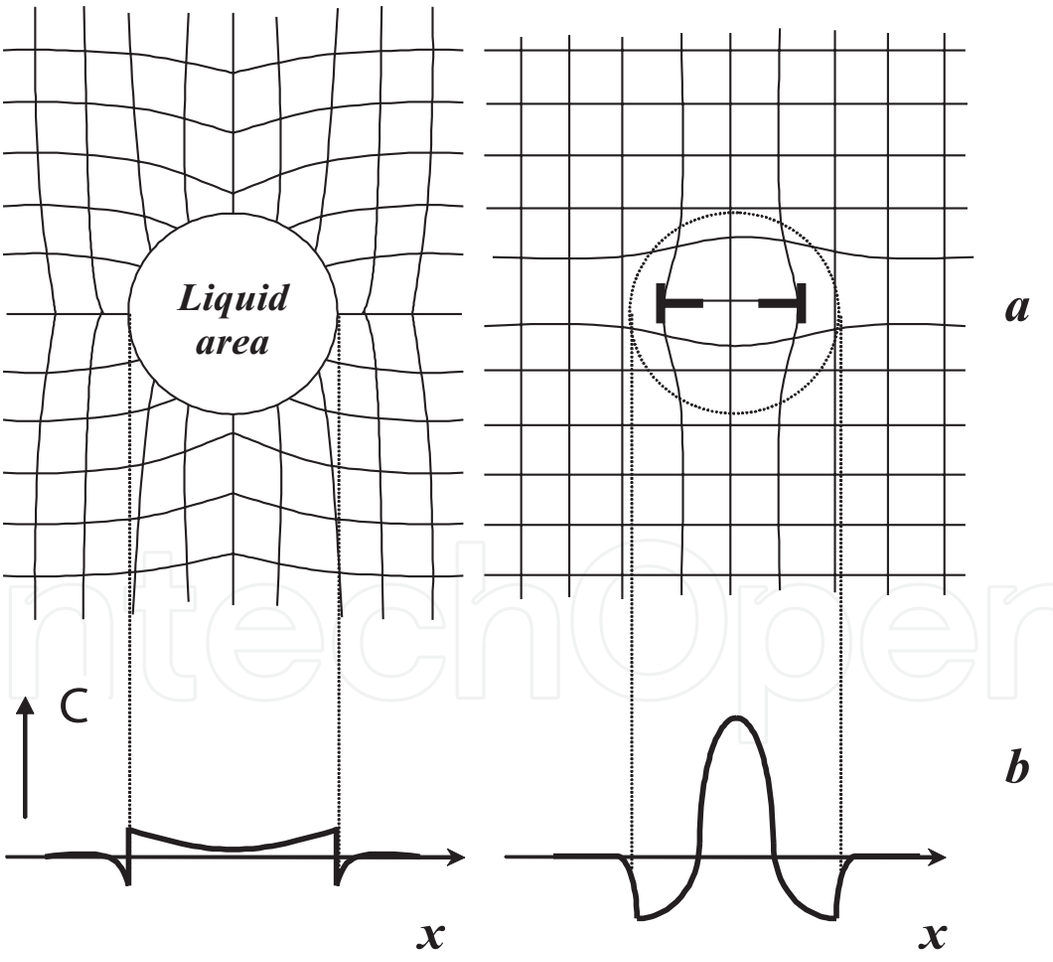

Figure 5. Diagram showing liquid-drop transformation into a dislocation [19]. (a) Lattice distortion and (b) impurity-concentration profile.

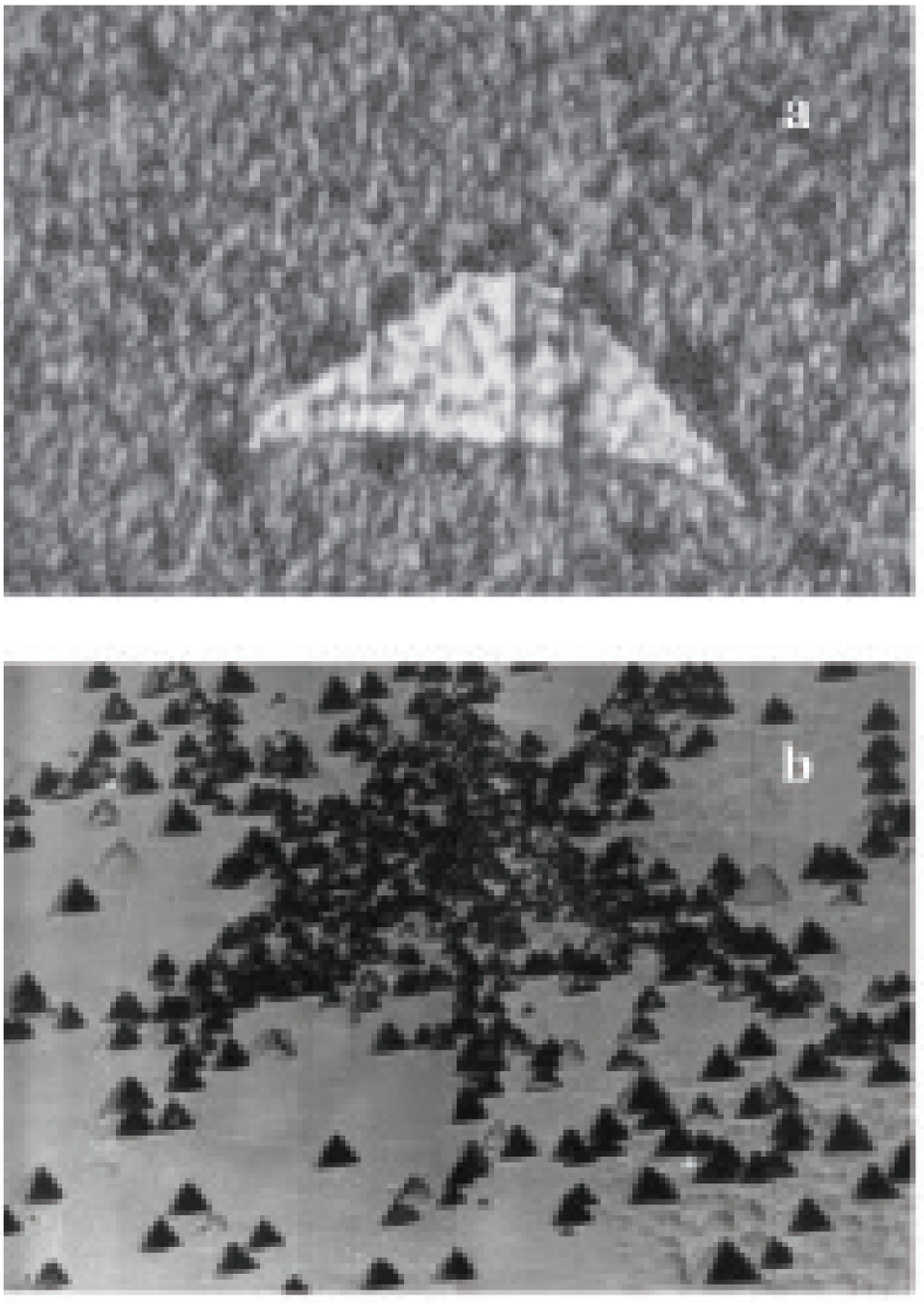

Figure 6. (a) photo of the surface of the polished section containing the Al-Si inclusion in silicon and (b) distribution of dislocation etch pits around the inclusion after four hours of annealing at j = 100 A/cm^2 and a temperature of 800°C. Polished section plane (111). 200× zoom.

4. Comparative analysis of the formation and electromigration of molten inclusions (AL-SI) in silicon and aluminum

In this context, the present investigation was aimed at an experimental study difference of the electromigration of melted Al-Si inclusions in silicon and aluminum crystals.

http://dx.doi.org/10.5772/67787

The experiments were performed in a setup that is schematically depicted in **Figure 7**. The samples had the form of silicon bars (4 × 4 × 15 mm; *n*-type, 20 Ω·cm, growth dislocation density not exceeding 4×10^3 1/m^2) and aluminum cylinders (length, 15 mm; diameter, 4 mm; average grain size, 500 μm). For investigations of the electromigration in silicon, a metal (Al) plate weighing 0.6–0.9 mg was placed between the {111} edge planes of silicon samples and the system was heated to a temperature above the eutectic (T = 850 K). The sample temperature was determined by the joint action of the external heater and the current passing through the sample. The temperature was measured by a thermocouple situated in the immediate vicinity of the sample.

For the formation of melted Al-Si inclusions in aluminum, particles of highohmic silicon with diameters of ~300–500 μm were placed into preliminarily made depressions on the edge surface of one aluminum cylinder. Then, the aluminum cylinders were matched with their edges, placed inside the quartz furnace tube (with a diameter of 5 mm), and pressed between the current carrying electrodes with graphite spacers. At temperatures above the eutectic, the components exhibited contact melting and formed melted film zones, which rapidly separated into separate drops (inclusions) with dimensions of 20–350 μm. These inclusions were always driven by the current (j =1.4 × 10^5 A/m^2) along the lines of electric field, but the velocity of this migration in both silicon and aluminum was dependent on the inclusion size l.

It was established that the formation of inclusions from a liquid film in silicon is accomplished during a 5–10 μm penetration of the melt into the crystal matrix volume, while in aluminum this process was accomplished within a 30–50μm thick layer. **Figure 8** shows micrographs of drifting Al-Si inclusions as observed after the electroannealing and crystallization.

Figure 8 shows the typical results as represented by the empirical plot of

$$W/j = a + b\ell, \tag{10}$$

where w/j is the specific migration velocity defined as the ratio of the velocity w of a melted inclusion to the current density j in the sample; a and b are empirical coefficients, the values of which are given in **Table 1**.

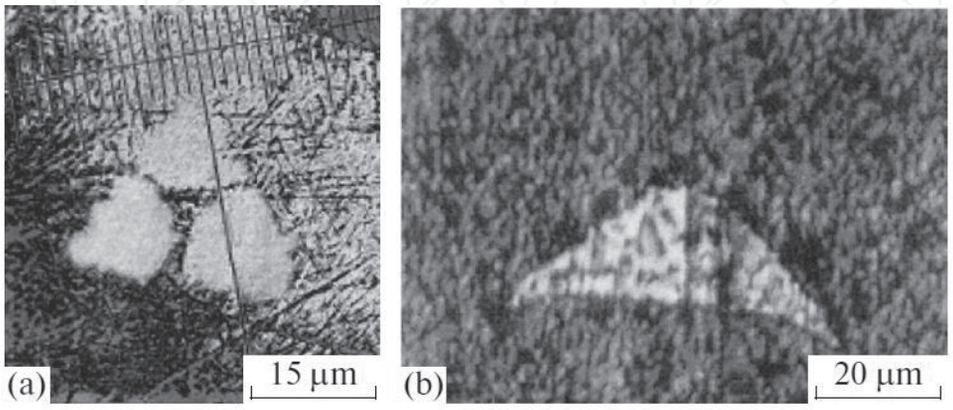

Figure 7. Micrographs showing Al-Si inclusions observed after electroannealing (j = 1.4 × 10^5 A/m^2) in (a) polycrystalline aluminum (T = 893 K) and (b) single crystalline silicon (T = 1043 K; section ⊥(111); magnification, ×200.

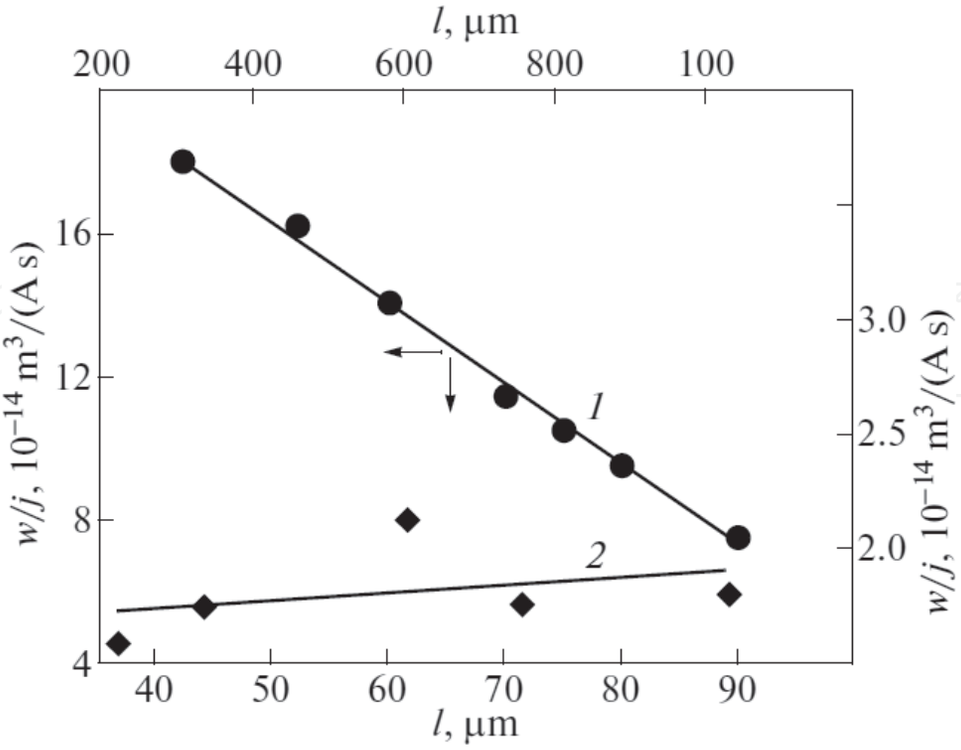

Figure 8. Plots of the specific migration velocity w/j versus size l of Al-Si inclusions in (1) silicon T = 1043 K and (2) aluminum at T = 893 K.

No	Parameter	Units	Temperature, K	
			1043	**893**
1.	Matrix material	–	Silicon	Aluminum
2.	Melt composition	$C_{Si}\backslash C_{Al}$, at%	76\24	10\90
3.	a, 10^{-14}	$m^3/(A{\cdot}s)$	27.4	1.7
4.	b	$m^2/(A{\cdot}s)$	-2.4×10^{-9}	2.2×10^{-12}
5.	P_t, 10^{-7}	Ω·m	36	4.5
6.	M, 10^{-3}	кg/mol	27	27
7.	V, 10^{-6}	m^3/mol	10.9	11.2
8.	L, 10^9	J/m^3	3.9	1.0
9.	λ	W/(m·K)	7.1	48
10.	δ	μm	200	200
11.	C, 10^{28}	$1/m^3$	5.5	5.4
12.	D, 10^{-9}	m^2/s	6.1	2.8
13.	Z^*	–	−1.1	−1.0
14.	P, 10^{-3}	V	230	−8.7

Table 1. Calculated and experimental data on the migration of melted Al-Si inclusions in polycrystalline aluminum and single crystalline silicon.

It was previously demonstrated that the transport of liquid inclusions in these systems is driven by two competitive mechanisms: thermoelectric phenomena (Peltier heat evolution) at interphase boundaries and electric field induced redistribution of components dependent on their effective atomic charges in the melt. The specific migration velocity w/j is proportional to the Peltier coefficient P of the crystal-melt interface and the effective charges Z^* of semiconductor and metal atoms in the eutectic melt.

We have described the migration of melted Al-Si inclusions in silicon and aluminum taking into account the condition $\beta\delta > D$ and data from the table, using Eqs. (7) and (10), and evaluating coefficients a and b from our experiments (**Figure 8**). The P and Z^* values were calculated using published data [11, 12] on the composition dependence of the resistivity of Al-Si melts; the heat conductivity was evaluated using the Wiedemann-Franz law. Since no data were available on the temperature dependence of the coefficient of mutual diffusion in Al-Si melts, the D values at e temperatures studied were taken from monographs [11, 13, 14]. The results of P and Z^* calculations for the electromigration of melted Al-Si inclusions are presented in **Table 1**.

An analysis of the obtained results allows us to ascertain that the electromigration of melted Al-Si zones in silicon, similar to the analogous processes in other semiconductors [8–11, 17, 18], is determined by the electromigration of melt components in the volume of inclusion and by the thermoelectric phenomena at interphase boundaries. The negative value of the effective charge on semiconductor atoms in the melt is indicative of their directed transport to the anode. This migration results in silicon depletion of the melt in the diffusion layer of the front part of the inclusion and silicon enrichment of the boundary layer in the trailing part of the melted zone. Accordingly, the electromigration favors the displacement of inclusions toward the negative electrode. An important feature of the obtained results (**Figure 8**, curve 1) is a clear manifestation of the mutually compensating contributions due to the P and Z^* values. A positive P value ensures evolution of the Peltier heat at the rear side of the inclusion and the absorption of this heat at the frontal boundary during the current passage. Therefore, under the action of thermoelectric factors, the inclusion must diffuse in the counter direction relative to the electric field lines. Moreover, this mechanism would predominate with increasing size of inclusions, which accounts for the fact that the electromigration and thermoelectric effects in experiments with silicon crystals appear as competitive (counteracting) factors.

As for aluminum, the size dependence of the specific migration velocity in this system is much less pronounced as compared to silicon, since the $P = P_S – P_L$ value (where P_S and P_L are the Peltier coefficients of the solid phase and melt, respectively) on the interphase boundary is also significantly smaller than in the semiconductor matrix and has the opposite sign ($P < 0$). For this reason, the motion of melted Al-Si zones in polycrystalline aluminum is also determined by the electromigration of Al atoms in the liquid phase and by thermoelectric effects, the role of which increases with the size of inclusions, but in this case the two mechanisms act complementarily to each other.

5. Conclusions

Thus, the electromigration of extrinsic zones in Si has been established to be determined by the dissolution-crystallization process at the interface between the solid and liquid phases. This

happens under the influence of Peltier heat localized at the phase interfaces and the forces of electric transport in the bulk inclusion. The size dependence of the inclusion displacement velocity, w, is shown to be governed by a linear law.

The contribution of electric transport and Peltier heat to the resulting velocity of zone displacement by the current is determined. It varies for inclusions of different sizes; all other conditions being constant, the contribution of electric transport decreases with the increase of inclusion thickness.

Acknowledgements

The author is grateful to Professor Anatoliy M. Orlov for the interest and support of this research area. This study was partially supported by the Ministry of education and science of the Russian Federation (project 8.5171.2017).

Author details

Arkady Skvortsov

Address all correspondence to: skvortsovaa@outlook.com

Moscow Polytechnic University, Moscow, Russia

References

[1] Perepezko J.H, Wilde G. Melt undercooling and nucleation kinetics. Current Opinion in Solid State and Materials Science. 2016; **20(1):** 3–12. DOI: 10.1016/j.cossms.2015.07.001

[2] Brassart L., Liu Q., Suo, Z. Shear, dilation, and swap: mixing in the limit of fast diffusion. Journal of the Mechanics and Physics of Solids. 2016; **96:** 48–64. DOI: 10.1016/j.jmps.2016.06.013

[3] Perepezko JH, Hoffmeyer MK, De Cicco MP. Analysis of melt undercooling and crystallization kinetics. Metallurgical and Materials Transactions A: Physical Metallurgy and Materials Science. 2015; **46(11):** 4898–4907. DOI: 10.1007/s11661-015-2970-9

[4] Tian Z, Lee S, Chen G. Heat transfer in thermoelectric materials and devices. Journal of Heat Transfer. 2013; **135(6):** 061605. DOI: 10.1115/1.4023585

[5] Sharmin A, Rashid M, Gaddipati V, Sadeque A, Ahmed S. Multiscale design of nanostructured thermoelectric coolers: effects of contact resistances. Journal of Electronic Materials. 2015; **44(6):** 1697–1703. DOI: 10.1007/s11664-014-3520-8

[6] Khripach NA, Papkin BA, Korotkov VS, Zaletov DV. Study of the influence of heat exchanger body design parameters on the performance of a thermoelectric generator for automotive internal combustion engine. Biosciences Biotechnology Research Asia. 2015; **12(Spl. Edn. 2):** 677–689. http://dx.doi.org/10.13005/bbra/2084.

[7] Liu D-W, Li J-F. Electrocrystallization process during deposition of Bi-Te films. Journal of the Electrochemical Society. 2008; **155(7):** D493–D498. DOI: 10.1149/1.2907398

[8] Rodbell KP, Shotynsky SR. Electromigration in sputtered Al-Si thin films. Thin Solid Films. 1983; **108:** 95–102. DOI: 10.1016/0040-6090(83)90045-7

[9] Skvortsov AA, Zuev SM, Koryachko MV, Glinskiy V. Thermal shock and degradation of metallization systems on silicon. Microelectronics International. 2016; **33(2):** 102–106. DOI: 10.1108/MI-05-2015-0049

[10] Orlov AM, Skvortsov AA. Temperature gradient effect on the electromigration of Ag-Te melt inclusions in tellurium. Inorganic Materials. 2007; **43(5):** 471–474. DOI: 10.1134/S0020168507050056

[11] Orlov AM, Skvortsov AA, Salanov AA. Electric transport in gallium antimonide single crystals involving molten GaSb-Sn inclusions. Semiconductors. 2004; **38(4):** 376–379. DOI: 10.1134/1.1734661

[12] Gershanov VYu, Garmashov SI. Non-stationary nonlinear effects at mass transfer in small volumes of solution in melt enclosed in anisotropic crystal. Journal of Crystal Growth. 2009; **311(9):** 2722–2730. DOI: 10.1016/j.jcrysgro.2009.01.080

[13] Magomedov MN. On self-diffusion and surface energy under compression of diamond, silicon, and germanium. Technical Physics. 2013; **58(12)**: 1789–1799. DOI: 10.1134/S1063784213120153

[14] Zhang J.-S., Wu Y.-P., Wang Y.-G., Tao Y. Thermomigration in micro interconnects in integrated circuits. Journal of Materials Science-Materials in Electronics. 2010; **21(10):** 1090–1098.

[15] Gottstein G. Physical Foundations of Material Science. Berlin-Heidelberg: Springer-Verlag. 2004. 347 p.

[16] Geguzin YaE, Kaganovskiĭ YS. Diffusive mass transfer in island films. Soviet Physics – Uspekhi. 1978. **21(7)**:611–629. DOI: 10.1070/PU1978v021n07ABEH005667

[17] Belashchenko DK, Orlov AM, Orlova SP. Crystallization of semiconductors in a constant electric field. High Temperature. 1976; **14(3):** 516–520.

[18] Orlov AM, Belashchenko DK, Derikova SA, Parkhomenko VI. Mechanism and kinetics of the mass transfer of impurities in polar A3B5 compounds. Soviet Physics Journal. 1976. **19(5):** 576–580. DOI: 10.1007/BF00952553

[19] Ravi KV. Imperfections and Impurities in Semiconductor Silicon. A. Wiley-Interscience Publication. 1981. 348 p.

IntechOpen